



# Design of lithium cobalt oxide electrodes with high thermal conductivity and electrochemical performance using carbon nanotubes and diamond particles



Eungje Lee <sup>a</sup>, Ruben Arash Salgado <sup>b</sup>, Byeongdu Lee <sup>c</sup>, Anirudha V. Sumant <sup>d</sup>, Tijana Rajh <sup>d</sup>, Christopher Johnson <sup>a</sup>, Alexander A. Balandin <sup>b</sup>, Elena V. Shevchenko <sup>d,\*</sup>

<sup>a</sup> Chemical Sciences and Engineering Division, Argonne National Laboratory, Argonne, Illinois 60439, USA

<sup>b</sup> Nano-Device Laboratory, Department of Electrical and Computer Engineering and Materials Science and Engineering Program, University of California - Riverside, Riverside, CA 92521, USA

<sup>c</sup> Advanced Photon Source, Argonne National Laboratory, Argonne, Illinois 60439, USA

<sup>d</sup> Center for Nanoscale Materials, Argonne National Laboratory, Argonne, Illinois 60439, USA

## ARTICLE INFO

### Article history:

Available online 28 December 2017

### Keywords:

Li-ion battery  
Carbon black-free  
Binder-free  
Current collector-free  
Thermal conductivity  
CNTs  
LiCoO<sub>2</sub>  
LCO  
Diamond

## ABSTRACT

Thermal management remains one of the major challenges in the design of safe and reliable Li-ion batteries. We show that composite electrodes assembled from commercially available 100 μm long carbon nanotubes (CNTs) and LiCoO<sub>2</sub> (LCO) particles demonstrate the in-plane thermal conductivity of 205.8 W/m<sup>2</sup>K. This value exceeds the thermal conductivity of dry conventional laminated electrodes by about three orders of magnitude. The cross-plane thermal conductivity of CNT-based electrodes is in the same range as thermal conductivities of conventional laminated electrodes. The CNT-based electrodes demonstrate a similar capacity to conventional laminated design electrodes, but revealed a better rate performance and stability. The introduction of diamond particles into CNT-based electrodes further improves the rate performance. Our lightweight, flexible electrode design can potentially be a general platform for fabricating polymer binder- and aluminum and copper current collector-free electrodes from a broad range of electrochemically active materials with efficient thermal management.

© 2017 Published by Elsevier Ltd.

## 1. Introduction

Since the first demonstration of Li-ion batteries based on layered TiS<sub>2</sub> cathode and metallic lithium anode in 1976 [1], it took about 15 years to release the first rechargeable commercial Li-ion battery [2]. Now rechargeable Li-ion batteries became common in consumer electronics and their popularity continues to grow for electric vehicle and aerospace applications. Such batteries have a number of attractive properties. They are lightweight; provide high energy density; and have low self-discharge. Recent progress in battery materials research allowed significant improvement in design of high energy density and high power Li-ion batteries [2–6]. However, the safety aspects of Li-ion batteries are still not properly addressed [2,7]. Transportation and grid-scale energy storage applications require high energy density battery systems

that are realized via assembly of large format cells into packs. Even though Li-ion batteries have high efficiency (~85–90%) in converting of the stored chemical free energy into electric work, still a certain amount of energy will be lost as a result of ohmic heating owing to the current flow through the internal resistance during operation of any battery [8–10]. In addition, thermodynamics of the chemical reactions during charging and discharging cycles, especially within the cathode materials can also contribute to heating events in Li-ion batteries [11–13]. While dendrite growth is a concern for anodes, especially in Li-metal batteries [14], the low thermal stability of the cathode material and its tendency to release pure oxygen, promoting combustion, when over-charged [2,15] impose safety problems for cathodes in Li-ion batteries. Overheating of the battery results in the performance degradation, decreased battery life, and more seriously, increased risk of fire or explosion. Another problem of the Li-ion battery is their temperature-dependent performance [12,16–19]. Therefore, thermal management becomes a serious issue that impedes the spreading of high energy density batteries for large-scale

\* Corresponding author.

E-mail address: [eshevchenko@anl.gov](mailto:eshevchenko@anl.gov) (E.V. Shevchenko).

applications [15].

The thermal management at the pack level can be achieved via circulating air or liquid heat transfer media around the battery packs. This active cooling approach is mainly applied to large scale electric automotive and aerospace applications since it requires complex, large, heavy, and expensive universal active cooling systems. For smaller electric vehicles and devices, it is more appropriate to utilize a passive cooling strategy that does not require cumbersome additional cooling systems. For example, cells can be surrounded by phase change materials (PCM) that absorb the generated heat in Li-ion cells and melt up upon heating. When cells cool off, the PCM hardens releasing the heat into the outside media. However, the poor thermal conductivity of PCM can result in slow heat dissipation which can create unfavorable thermal regime for battery operation [20]. Combination of PCM and aluminum heat transfer matrix is suggested to improve the low heat conductivity of the PCM.

Besides thermal management at the pack level, there are more direct approaches to improve the safety of batteries at the individual cell level. It has been known that the poor heat transfers across the interface of a cathode and a separator limits the heat dissipation, and the heat built up at the interface region causes the decomposition of solid electrolyte interface and shortage of the circuit as a result of separator failure [21]. Therefore, multilayer separators, ceramic particle coatings and thermoresponsive polymers that decrease conductivity due to expansions upon heating have been adopted to prevent the catastrophic failures by permanent shut down of the battery in the event of overheating [7]. Therefore, a great number of interesting ideas have been considered to minimize the consequences of battery failure with the assumption that the conventional design of the electrodes remains unchanged.

The conventional design of the electrodes in Li-ion battery is based on the laminated composite film, which consists of electrochemically active material, carbon black conducting agents, and polymer binder, coated on metal foil current collector [22]. Such electrode design is proved to be effective for achieving good electrochemical performance and for mass production. Even with small loadings, the carbon black takes large volume fraction in the structure of conventional cathode electrodes and plays a critical role in creating good electrical connections between the active material particles and the aluminum current collector. However, the carbon black is a poor thermal conductor. The low thermal conductivity of the carbon black, which is typically in the range between  $\sim 0.1$  and  $1 \text{ W/m}^2\text{K}$  at room temperature, is the main reason for the overall low heat dissipation property of the conventional cathode electrodes [23,24]. Moreover, the electrodes fabricated via conventional laminate process have high porosity and a granular microstructure that are not optimal for fast thermal conduction. Poor thermal conductivity may also create thermal and electrical gradients within the electrodes that can lead to locally unbalanced states of charging and discharging (i.e., local overcharging and discharging) [25]. It is noteworthy that the dry conventional cathode electrodes demonstrate thermal conductivity in the range between  $0.27 \text{ W/m}^2\text{K}$  and  $0.79 \text{ W/m}^2\text{K}$  [26–28]. The wetting of the dry electrode with electrolyte and interfacing it with aluminum foil can increase the thermal conductivity up to  $8.23 \text{ W/m}^2\text{K}$  [27]. In the light of raising concerns of thermal management for safer Li-ion batteries, it is imperative to consider alternative approaches of electrode assembly that can provide material-level thermal management solution without compromising the electrochemical performance.

A possible approach for addressing the low thermal conductivity issue is to replace the carbon black with other carbon allotropes that have better intrinsic thermal conductivity. In this

scenario, graphene [29] and carbon nanotubes (CNTs) [30,31], have become promising alternatives for the design of the electrode matrix [32]. The concept of using different carbon allotropes such as graphene, CNTs and fibrous carbon aerogels has been explored in order to fabricate binder free, flexible electrodes for Li-ion batteries [33,34] and Zn-air batteries [35]. The high quality single layer graphene reveals thermal conductivity in the range from  $2000 \text{ W/m}^2\text{K}$  to  $5000 \text{ W/m}^2\text{K}$  [29]. The graphene based structures obtained by annealing of graphene oxide demonstrated thermal conductivities of  $\sim 61 \text{ W/m}^2\text{K}$  [36]. The thermal conductivity of the reduced graphene oxide is lower than that of graphene owing to the high concentration of defects, structural disorder and relatively small size of  $sp^2$  domains. However, composites assembled from extended graphene monolayers can present a challenge for electrolyte diffusion due to the lodging of the pores [37]. In turn, thermal conductivity of individual CNTs was experimentally reported to be in the range from  $1750 \text{ W/m}^2\text{K}$  to  $5800 \text{ W/m}^2\text{K}$  [38]. The electrical conductivity of compacted CNT structures was found to be even higher than that of the compacted graphene structures [39]. Generally speaking, both CNTs and graphene offer excellent electrical and thermal conductivities attractive for Li-ion battery applications. However, most of the studies on the alternative electrode designs utilizing carbon allotropes focus mainly on the electrochemical and mechanical aspects of the batteries and only limited number of studies discuss the thermal management aspects [32,34].

Previously, various types of binder-free electrode designs have been suggested. However, most of them are only applicable to nano-scale active materials, such as nanoparticles [40,41], nanowires [42–44], and hierarchical structures [45,46]. Hasegawa et al. [47] demonstrated moderate performance of binder-free  $\text{LiCoO}_2$  electrode prepared with CNT (less than 10 wt%). However, their  $\text{LiCoO}_2/\text{CNT}$  composite electrodes without current collector indicated significant rise in cell impedance particularly at high current density. Herein, we report on thermal conductivity and electrochemical performances of free-standing  $\text{LiCoO}_2/\text{CNTs}$  composite electrodes without using carbon black, polymeric binder, and Al foil current collector. The novel composite electrodes demonstrated excellent lateral thermal conductivity up to about  $205.8 \text{ W/m}^2\text{K}$ , which is three orders of magnitude higher than the thermal conductivity of the conventional laminated electrodes, without compromising specific capacity of  $\text{LiCoO}_2$ . The rate capability and deep cycling stability of the composite electrodes are even better than those of the conventional laminated electrode. We also discuss the effect of micron sized diamond particles and diamond nanoparticles on the thermal conductivity and electrochemical properties of the  $\text{LiCoO}_2/\text{CNT}$  composite electrodes.



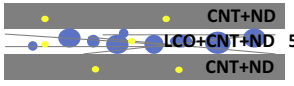

## 2. Experimental section

### 2.1. Materials and sample preparation

$\text{LiCoO}_2$  (LCO) particles were purchased from Sigma-Aldrich and used without any further modification/optimization. We used c-grade multi-walled CNTs purchased from NanoTechLab ( $\geq 95\%$  purity,  $100 \mu\text{m}$  long, diameter of CNTs is in the range of  $5\text{--}30 \text{ nm}$ ). The nanosized ( $\sim 2.3 \text{ nm}$ ) diamond and micron-sized ( $\sim 8\text{--}16 \mu\text{m}$ ) diamond powder samples were obtained from International Technology Center, Raleigh and NC Diamond Innovations, respectively. All samples for thermal conductivity and electrochemical tests were obtained by vacuum filtration of corresponding solutions through the filter such as microporous glass fiber filter (Wachman GF-F). Table 1 provides the information on the amounts of materials used for different types.

Corresponding amounts of materials were dispersed in  $250 \text{ mL}$

**Table 1**  
Description of the control CNT and composite CNT-based LCO electrodes.

| Description of electrodes  | Abbreviation | Composition and weight, mg  |
|--|--------------|---|
| Control CNT electrodes   | CNT          |  CNT 10.2783  |
| Three-layered electrodes. LCO is mixed with CNTs and sealed between two layers of CNTs.  | CNT-LCO      |  CNT 4.1575<br>LCO+CNT 51.7033+1.9770<br>CNT 3.9595                               |
| Three-layered electrodes. LCO is mixed with CNTs and sealed between two layers of CNTs. Each layer contains similar amount of nanodiamonds.          | CNT-LCO-ND   |  CNT+ND 4.2467+1.3800<br>LCO+CNT+ND 51.7573+2.0268+1.3949<br>CNT+ND 3.7902+1.5041 |
| Three-layered electrodes. LCO is mixed with CNTs and sealed between two layers of CNTs. Each layer contains similar amount of micron sized diamonds. | CNT-LCO-MD   |  CNT+MD 3.9954+1.5508<br>LCO+CNT+MD 51.7800+2.0598+1.4598<br>CNT+MD 4.1151+1.4258 |

of isopropyl alcohol (IPA) and sonicated for 20 min. CNT-LCO, CNT-LCO-ND and CNT-LCO-MD samples have three-layered design in which the middle layer containing LCO particles was sandwiched between two layers of CNTs papers. Control CNT sample was obtained via filtration of suspension of 10.2783 mg of CNTs dispersed in 250 mL of isopropanol. After that the suspension of CNTs was filtrated by vacuum forming a black CNT paper on the filter. After the filtration, all samples were annealed in an oven at 200 °C for 12 h and further used in electrochemical tests without any additional processing. Typical LCO loading was 5.4 mg/cm<sup>2</sup>. The SEM imaging of the samples was carried out using JEOL 7500F scanning electron microscope.

For comparison, conventional laminated electrodes were prepared by coating aluminum foil (20 μm thick) with a slurry containing 84 wt% of LCO (Sigma-Aldrich) powder, 8 wt% of carbon black powder (Super-P, Cabot Co.), and 8 wt% of polyvinylidene fluoride binder (binder) in a N-methyl-2-pyrrolidone (NMP) solvent. The typical LCO loading was 5.0 mg/cm<sup>2</sup> and the thickness of electrode film (excluding Al foil) was 50 μm.

## 2.2. Electrochemical testing

In all electrochemical tests, the samples were used directly after annealing. Electrochemical tests were conducted on 1.27 cm in diameter samples punched from 3.5 cm in diameter samples obtained by filtration. The battery cycling tests were performed with the 2032 coin type cells with Li metal foil as the counter electrodes and 1.2 M lithium hexafluorophosphate (LiPF<sub>6</sub>) in ethylene carbonate/ethyl methyl carbonate (3:7 weight ratio) electrolyte (Tomiyaama). Half-cell cycles were operated at 0.5 C-rate (1C-rate = 140 mA/g) between 2.75–4.2 and 2.75–4.5 V vs. Li/Li<sup>+</sup> voltage ranges, using an automated Maccor 2000 battery tester. The rate performance study on electrodes was conducted with cycling the coin cells between 2.75 and 4.2 V vs. Li/Li<sup>+</sup> voltage range at 0.2C, 0.5C, 1C, 2C and 3C discharge rates while the charge rate was kept at 0.2C. All of the coin cell tests were conducted in environment chamber set at 25 °C.

## 2.3. Thermal measurements

The in-plane thermal conductivity was measured using the transient planar source technique (Hot Disk, TPS2500). For these measurements, an electrically insulated flat nickel sensor with a radius of 0.5 mm is sandwiched between two identical parts of the same sample. The sensor acts as the heat source and temperature

monitor, simultaneously. Thermal conductivity (*K*) of the material is determined by recording the temperature rise as a function of time using the equation  $\Delta T(\tau) = P(\pi^2 r K)^{-1/2} D(\tau)$ , where  $\tau = (t_m \alpha / r^2)^{1/2}$ ,  $\alpha$  is the thermal diffusivity,  $t_m$  is the transient measurement time,  $r$  is the radius of the sensor,  $P$  is the input heating power, and  $D(\tau)$  is the modified Bessel function. The time and the input power were chosen so that the heat flow is within the sample boundaries and the temperature rise of the sensor is not influenced by the outer boundaries of the sample. The TPS system was calibrated with the 3- $\omega$  method, a widely known standard technique for thermal conductivity measurements of thin films. Before each test, TPS system was also calibrated by testing a referenced silicon wafer.

The cross-plane thermal conductivity was measured using an optical “laser flash” technique (LFA, Netzsch LFA 467). The method is compliant with the international standards ASTM E-1461, DIM E-821 and DIN-30905. In this technique, in order to measure the thermal diffusivity, each sample is placed into a stage, a xenon flash lamp produces shots with an energy of 10 J/pulse on the sample surface while the temperature rise is monitored at the other end with an infrared detector. The thermal conductivity is determined from the equation  $K = \rho \alpha C_p$ , where  $\rho$  is the mass density, and  $C_p$  is the specific heat of the sample measured separately. The details of the thermal measurement procedures were previously reported [36,48,49]. Prior to the measurements on CNT-based samples thermal conductivities of the standards were measured by Hot Disk and LFA (Table 2). The thermal conductivities obtained for standards at room temperature are in agreement with their tabulated values. Note, that Hot Disk and LFA require different materials as standards.

## 3. Results and discussion

As described in the experimental section, all electrodes tested in

**Table 2**  
Thermal conductivity of different materials (standards) measured by LFA and Hot Disk at 25 °C.

| Test     | Material             | kW/m <sup>2</sup> K | ±    |
|----------|----------------------|---------------------|------|
| LFA      | Pyroceram            | 4.01                | 0.04 |
| LFA      | Pyrex                | 1.01                | 0.03 |
| LFA      | Poco-graphite AXM-5Q | 91.7                | 0.02 |
| Hot disk | Stainless Steel      | 13.48               | 0.03 |
| Hot disk | Silicon              | 143.86              | 0.03 |

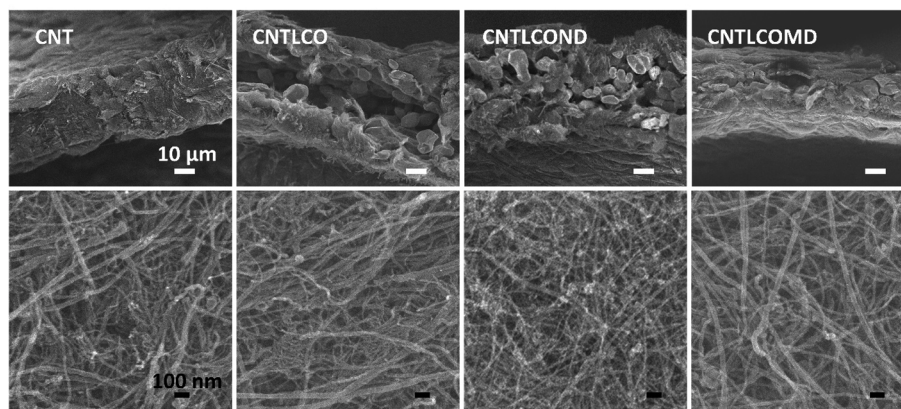


Fig. 1. SEM images of cross-plane (top) and lateral plane (bottom) of control CNT and composite CNT-LCO, CNT-LCO-ND and CNT-LCO-MD electrodes.

our study were obtained via filtration of suspensions of CNTs and CNTs mixed with LCO particles [50–52]. The suspensions were prepared via sonication of solid precursors in isopropanol. The formation of a stable suspension is a critical step that further determines the thermal and electrochemical performance of the fabricated electrodes. It is worth mentioning that in our previous work while the electrochemical performance of electrodes poly-disperse CNT-based composites of iron oxide nanoparticles was good, the electrochemical performance of CNT-based electrodes assembled from commercially available  $\text{Li}[\text{Ni}_{1/3}\text{Co}_{1/3}\text{Mn}_{1/3}]\text{O}_2$  was significantly compromised. As we recently figured out it could be a result of poor dispersibility of  $\text{Li}[\text{Ni}_{1/3}\text{Co}_{1/3}\text{Mn}_{1/3}]\text{O}_2$  particles in isopropanol that limited the interfacing of CNTs and particles of electrochemically active materials. In order to address this issue, we increased the volume of isopropanol and duration of sonication up to 250 mL and 20 min, respectively. We found that these conditions were sufficient to obtain a relatively stable CNTs and CNTs mixed with LCO dispersions resulting in more uniform electrodes. No conductive agents, polymer binders and metal current collectors were used to fabricate the composite electrodes and CNT matrix served as a current collector. Sandwiching of electrochemically active cathode layer (in this study, LCO mixed with CNTs) between two thin layers of CNTs is important for the robust performance of the composite electrodes in electrochemical tests. In case when electrochemically active material interfaces the electrolyte directly (no external CNTs layers), the fading of the performance was observed as a result of delamination of LCO particles from the electrode matrix.

In our previous work, we observed high thermal conductivities for composite electrode based on polydisperse CNTs [51]. Taking into account that nowadays CNTs of controlled length are

commercially available, we decided to explore the effect of the CNT length on the thermal conductivity and electrochemical performance. Since the electrochemical performance of electrodes fabricated from short, 5–20  $\mu\text{m}$  long CNTs was fading abruptly, we focused on electrochemically stable composite electrodes assembled from long, 100  $\mu\text{m}$  CNTs.

Expecting that the cross-plane thermal conductivity in CNT-based composite LCO electrode (CNT-LCO sample) can be limited by the relatively small number of the CNTs contacts across the electrode we explored the possibility of cross-plane heat transfer enhancement by the introduction of particles of materials with high thermal conductivity. Bulk diamond has an excellent thermal conductivity of 2200  $\text{W}/\text{m}^{\circ}\text{K}$  [30,31], and hence we investigated the effect of nano- and micron-sized diamond particles on the in-plane and cross-plane thermal conductivities in composite electrodes (samples CNT-LCO-ND and CNT-LCO-MD, respectively). While the thermal conductivity of micron and nanosized diamond may be lower than that of bulk diamond due to the phonon-boundary scattering [53–55], it is expected to be still much higher than the thermal conductivities of conventional electrode materials. The detailed description of the LCO/CNT composite electrodes is given in Table 1.

The scanning electron microscopy (SEM) analysis revealed that CNTs were rather entangled and randomly oriented in lateral planes; however, the majority of CNTs have preferred in-plane orientation (Fig. 1). The average thicknesses of the CNT, CNT-LCO, CNT-LCO-ND and CNT-LCO-MD samples were  $\sim 30 \mu\text{m}$ , 45  $\mu\text{m}$ , 35  $\mu\text{m}$  and 33  $\mu\text{m}$ , respectively. In case of three layered electrodes such as CNT-LCO, CNT-LCO-ND and CNT-LCO-MD samples the thickness of top and bottom CNT layers was  $\sim 7\text{--}8 \mu\text{m}$ . The individual CNTs were predominantly aligned parallel to the filter.

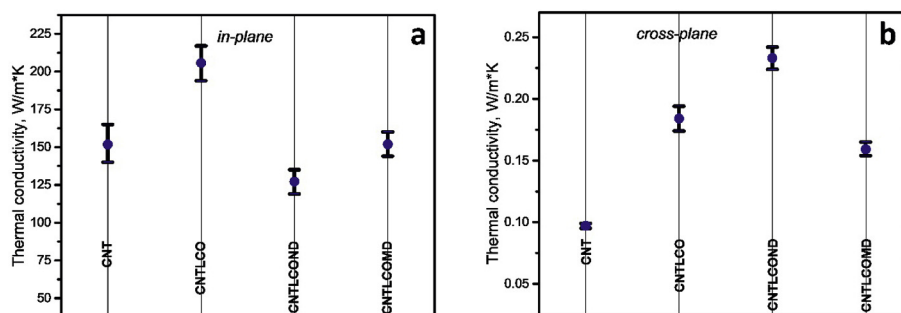
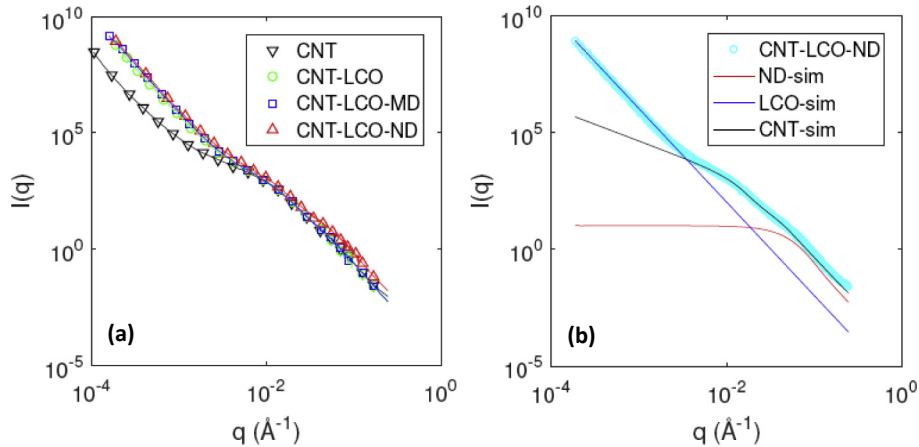


Fig. 2. Comparison of the room temperature in-plane (a) and cross-plane (b) thermal conductivities of CNT only sample and those of  $\text{LiCoO}_2/\text{CNT}$  composite electrodes as is (CNT-LCO) and with incorporated nano- and micro-sized diamond particles (CNT-LCO-ND and CNT-LCO-MD, respectively).





**Fig. 3.** (a) SAXS patterns measured on composite CNT-LCO, CNT-LCO-ND and CNT-LCO-MD and control CNT samples; (b) structure factors from individual components CNTs, LCO particles and nanodiamonds.

Fig. 2 gives the in-plane and cross-plane thermal conductivities for the CNT-based LCO electrodes and reference CNT sample. The in-plane thermal conductivity was measured using Hot Disk technique that allows fast and consistent measurements of thermal transport properties data without the influence of thermal contact resistance and well suited for samples with high degree of anisotropy in the sample structure. However, since the thicknesses of the samples was close to the lowest limit for sample thickness imposed for Hot Disk technique, the cross-plane thermal conductivity was measured using Laser Flash technique (Netzsch LFA 467) that allows to measure thermal conductivity of thin films [48].

The CNT-LCO sample showed excellent in-plane thermal conductivity of 205.8 W/m<sup>2</sup>K. According to the recent studies the thermal conductivity of a conventional electrode is in the range of 0.27–0.79 W/m<sup>2</sup>K, which is much lower than that of the CNT-based electrodes observed here [26–28]. Despite of the high thermal conductivity of Al foil used as current collector, the overall thermal conductivity of the electrode interfacing with aluminum has been measured to be around 8 W/m<sup>2</sup>K [27]. Even lower thermal conductivity of 3 W/m<sup>2</sup>K has been reported for whole cell [20]. Therefore, the in-plane thermal conductivity of CNT-LCO sample is up to three orders of magnitude higher than the thermal conductivity of dry conventional laminated electrodes, and as high as that of bare aluminum (205.0 W/m<sup>2</sup>K) that is used as a heat transfer matrix in the PCM-based passive cooling systems. Note, the thermal conductivity of LiCoO<sub>2</sub> is around 5.4 W/m<sup>2</sup>K m<sup>-1</sup> K<sup>-1</sup> [56].

The cross-plane thermal conductivity of CNT-LCO was 0.18 W/m<sup>2</sup>K that is in the range dry conventional laminated electrodes [25]. The significant difference in the in-plane and cross-plane thermal conductivities observed for CNT-based samples is expected for highly anisotropic materials [31,32]. Interestingly, both the in-plane and cross-plane thermal conductivities of the composite CNT-LCO sample were significantly higher than that of control sample consisting of CNT bundle only. Although the analysis of mass density of the samples and their microstructure have not allowed us to establish a strict correlation of these parameters with the thermal conductivity, it is presumed that higher thermal conductivity values in the CNT-LCO sample results from the lower disorder, better in-plane alignment of CNTs in these specific samples and coupling between individual CNTs and LCO particles. One should note that individual CNTs have the thermal conductivity in the range from 3000 W/m<sup>2</sup>K to 3500 W/m<sup>2</sup>K at room temperature [38]. The thermal conductivity of CNT bundles can vary in a wide range depending strongly on the sample microstructure and method of

preparation.

Aiming to further improve thermal conductivity (especially the cross-plane one) we investigated the effect of nano- and micron-sized diamond particles on the thermal conductivity in the CNT based composite electrodes. We added the same amount of nano- (ND) and micron- (MD) sized diamonds to the corresponding samples. However, we observed the decrease in the in-plane thermal conductivity in both CNT-LCO-ND and CNT-LCO-MD samples as compared to CNT-LCO sample (Fig. 2). The reduction in the in-plane thermal conductivity can be explained by additional scattering for phonons propagating in individual CNTs by attached diamond particles [57]. However, in the case CNT-LCO-ND, we observed an increase in the cross-plane thermal conductivity most likely due to better coupling in the cross-plane direction introduced by the diamond particles. The obtained results suggest that the arrangement of CNTs and their connectivity are the key factors that determine the thermal conductivity. The cross-plane thermal conductivities of the composite electrodes fabricated from long, 100  $\mu\text{m}$  CNTs in this study are substantially lower than the cross-plane thermal conductivity of previously reported CNT based electrodes that were assembled from polydisperse CNTs [51]. Therefore, we attribute the low cross-plane thermal conductivity observed in this study to more pronounced lateral arrangement of nanotubes in the samples prepared from longer CNTs. Our results do not completely rule out the use of nano- and micro-diamond particles for improvement of the thermal management of the battery electrodes but rather emphasize the need in optimization of the diamond particles size and their coupling to other filler materials.

Small-angle X-ray scattering (SAXS) was used to evaluate the morphological nature of the CNT-based structures. The results indicated that all three composite electrodes have similar scattering patterns (Fig. 3a). According to SAXS data, the average radius of individual multiwall CNTs is 12.4 nm. The radius of nanodiamonds is found to be 2.3 nm with 1 nm distribution width. In all samples no structure factor of CNTs is found indicating that CNTs are separated from each other and no bundles of CNTs are formed. Fig. 3b shows the scattering from LCO, CNTs and nanodiamonds in the composite electrodes. We estimated from scattering data the number ratio of CNTs and nanodiamonds (ND), assuming their densities as 1.5 and 3.52 g/cm<sup>3</sup> [58], respectively, as  $\sim 420$  nanoparticles per 1 nm length of single CNT. This number is supported by good agreement of the experimental scattering data and simulated curve based on individual scattering factors in the CNT-LCO-

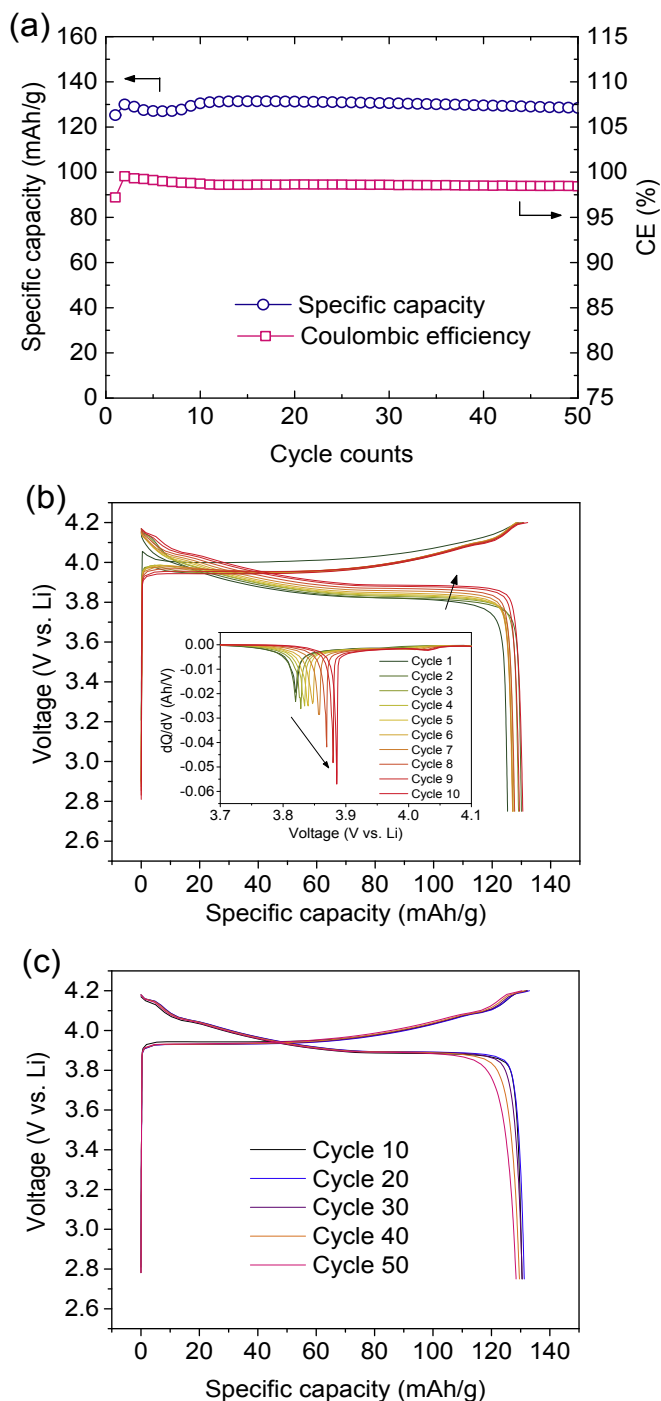


**Fig. 4.** Electrochemical performance of Li/CNT-LCO cell cycled between 2.75 and 4.2 V at 0.5C-rate (70 mA/g): (a) cycle performance, and voltage profiles for (b) initial 10 cycles and (c) after the 10th cycle. Inset of (b) shows shift of dQ/dV peak during initial 10 discharge cycles.

ND sample. The scattering from macrodiamonds (MD) is not noticeable in the SAXS data, indicating that their concentration is marginal as compared to LCO or CNTs. This, in turn, confirms that the same amount of nano-sized particles leads to the huge difference in the number ratio between CNTs diamond particles depending on their size. The absence of the structure factors for all components in composite electrodes confirms their random mixing without any phase separation. The SAXS data indicating the good mixing of CNT and LCO particles are also supported by the fact that

CNTs facilitate the dispersion of LCO in isopropanol indicating the interactions between CNTs and LCO particles. Indeed, being mixed with isopropanol, micron sized LCO particles tended to transition into suspension more efficiently in the presence of CNTs.

Fig. 4a shows the electrochemical cycling data of the CNT-LCO composite electrode. The CNT-LCO sample demonstrates good specific capacity (~130 mAh/g) and capacity retention when cycled between 2.75 and 4.2 V at 70 mA/g. Interestingly, the CNT based composite electrodes require initial formation cycles before the stable performance was reached (~10 cycles as shown in Fig. 4a). This effect is likely due to the electrode experiencing decreasing polarization. Fig. 4b shows the fluctuating specific capacity and decreasing polarization during the initial 10 cycles of the Li/CNT-LCO cell. The decreasing polarization during the initial 10 cycles is clearly represented by the shift of discharge dQ/dV peaks to higher voltage, as shown in the inset of Fig. 4b. After the conditioning steps, stable voltage profiles were observed. The gradual capacity drop was observed mainly in the voltage range between 3.9–3.6 V (Fig. 4c) while overall capacity of the CNT-LCO retention after 70 cycles was ~98% (Fig. 4a). While all types of electrodes demonstrated very similar stability in the 2.75–4.2 V cycling range, CNT-LCO performed the best in 2.75–4.5 V cycling range (Fig. 5). The CNT based electrodes modified with the performance as compared to the CNT-LCO. The electrochemical oxidation (EO) of the organic electrolyte resulting in the growth of thick passivation layer at the interface of the active cathode material is identified as one of reasons responsible for the capacity loss in Li-ion batteries. Higher voltage (above 4.1 V) is known to promote EO [59]. Lower stability in high voltage cycling range of the electrodes modified with diamond particles can be attributed to smaller contact area between LCO particles and CNTs as a result of diamond particles adhered to the surface of CNTs, and hence, it can lead to higher degree of LCO surface degradation during EO in the high voltage range. We assume that interfacial of LCO with CNTs helps to slow down or minimize the deposition of passivation layer at the surface of LCO. The lower performance of the CNT based electrodes modified with diamond particles as compared to the CNT-LCO electrode can be tentatively attributed to the higher porosity of the diamond modified electrodes. Since the degradation of LCO takes place from the particle surface at above 4.2 V, higher porosity of the diamond containing samples may lead to the faster degradation of LCO. It has been well known that the high voltage stability of LCO particles can be substantially improved by surface coatings [60–64]. The capacity retention demonstrated by the CNT-LCO electrode fabricated from untreated LCO particles is comparable to that of optimized, coated LCO laminated electrodes [61,65,66]. We presume that the LCO particles are better electrically connected with CNTs in the CNT-LCO electrode and, as a result, the CNT-LCO has better current distribution on the electrode with less locally overcharged regions. Fig. 6 demonstrates much better rate performance for the CNT-based electrodes as compared to the conventional laminated electrodes. First principle calculations revealed large charge transfer between Li-ions and diamond surface resulting in their high-binding energy toward the diamond surface [14]. Thus we assume that better rate performance of electrodes modified with diamonds can be associated with strong preferential adsorption of Li-ions on the nanodiamond surface that results in the concentrating of Li-ions in the vicinity of the LCO.

#### 4. Conclusions

In this study we explored the use of multi-walled CNTs, micron sized diamond particles and diamonds NPs for design of cathodes with high thermal conductivity and good electrochemical

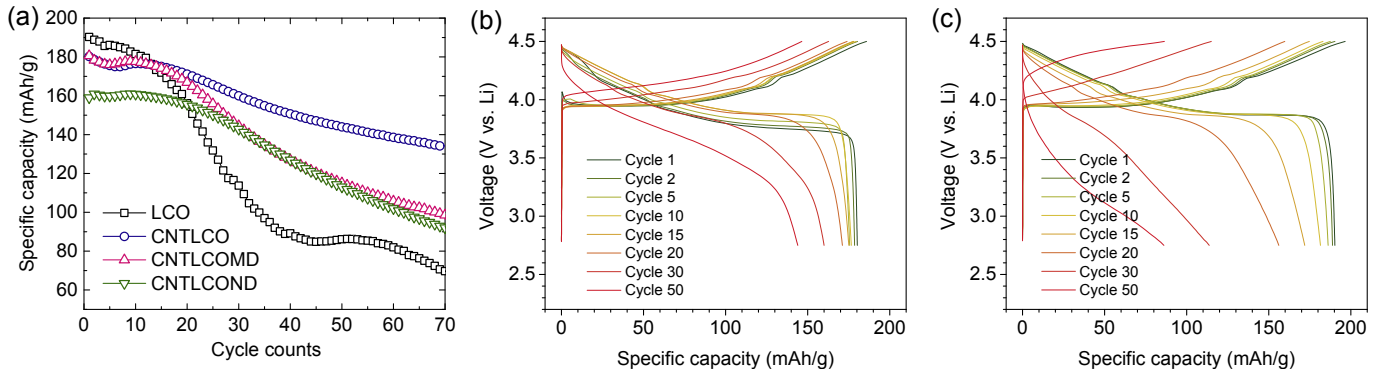


**Fig. 5.** Electrochemical performance of CNT-based and conventional electrodes cycled between 2.75 and 4.5 V at 0.5C rate (70 mA/g): (a) cycle performance, and voltage profiles for (b) CNT-LCO and (c) conventional LCO electrodes.

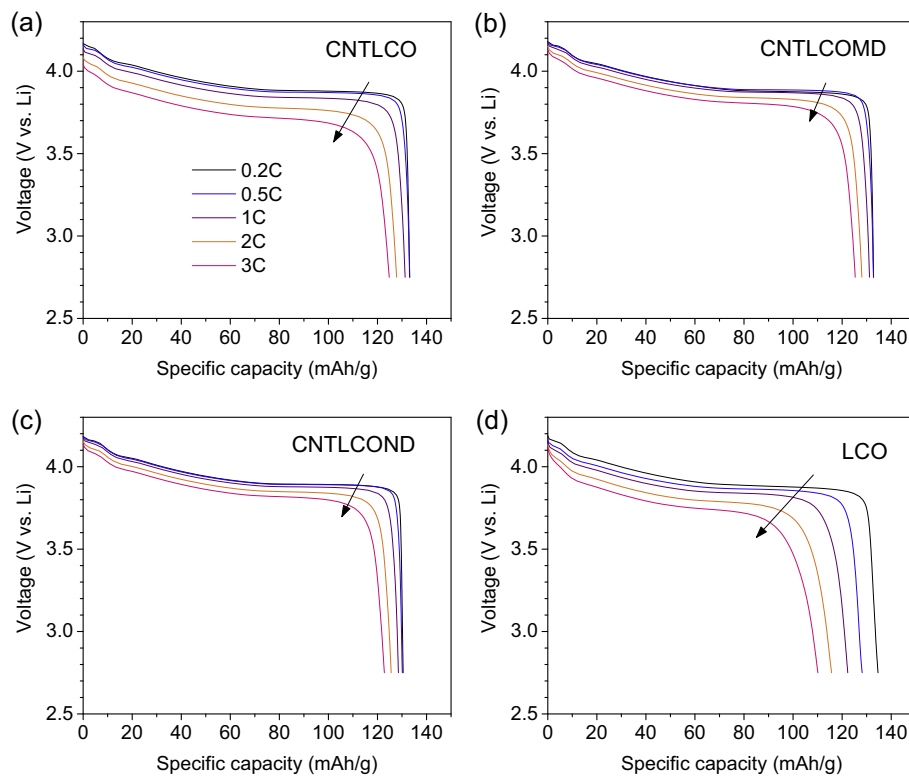


**Fig. 6.** Rate performances comparison of CNT-based and conventional LCO electrodes cycled between 2.75 and 4.2 V at different discharge rates (1C = 140 mA/g). Charge rate was fixed at 0.2C.

performance. We have shown that electrodes fabricated from commercial LCO particles and long ( $\sim 100 \mu\text{m}$ ) multi-walled CNTs in free standing configuration (without Al current collector) demonstrated excellent in-plane thermal conductivity of  $205.8 \text{ W/m}^2\text{K}$ . This value is comparable to that of aluminum itself and exceeds the thermal conductivity of dry conventional laminated electrodes by about three orders of magnitude. The cross-plane thermal conductivity of dry CNT-based LCO electrodes was in the range between  $0.16 \text{ W/m}^2\text{K}$  to  $0.23 \text{ W/m}^2\text{K}$  is in the range of thermal conductivities of conventional laminated electrodes. Furthermore, the electrochemical performance of CNT-based LCO electrodes is found to exceed that of conventional electrodes in terms of rate performance and high voltage cycling stability. It is also revealed that the length of CNTs and their arrangement are the important factors that determine the electrochemical performance and

thermal conductivity of the composite electrodes. The addition of diamond particles did not show significant enhancement in thermal conductivities, however allowed improvement in the rate performance of the electrodes. This observation in combination with recently reported suppression of Li dendrite growth in the presence of diamond NPs [14] highlight the promising properties of carbon allotropes that were not previously considered for energy storage systems.

There is also a number of additional potential advantages of the CNT-based electrode design besides the electrochemical performance and thermal conductivity discussed in this study. First of all, the removal of metal foil current collector will allow significant improvements in gravimetric energy density. For example, Al foil current collector accounts for up to 24 wt % of the total weight of the cathode in an automotive Li-ion battery [67]. The CNT-LCO

electrode tested in this study has LCO loading density of 1.2–1.6 g/cm<sup>3</sup>. This number obtained for electrodes in research laboratory is not much less than that of commercial LCO electrodes with 2.5 g/cm<sup>3</sup> LCO loading accounted for 20 μm thick Al current collector (assuming 3.5 g/cm<sup>3</sup> LCO loading with no Al foil) [68]. The observed high rate performance of the CNT-LCO electrode as compared to that of the baseline laminated electrode (with typical for research studies LCO loading accounted for Al foil of ~0.7 g/cm<sup>3</sup>) [63,69,70] suggests further improvement in the active materials loading density without compromising performances. Second, the CNT-based electrode design can be also promising in cases when electrolyte reacts with current collector material or binding agent. Lastly, the flexibility of the CNT-based electrodes can offer more freedom in design of Li-ion cells and allows their utilization in flexible electronic devices.

Mass production of CNTs and graphene with well controlled properties is currently available and hence there is no barrier to start considering the replacement of carbon black with other forms of carbon that can provide advanced functions. We believe that the CNT-based electrode design is a promising approach towards high-performance, high-safety Li-ion batteries, and further optimization is currently being pursued.

### Conflicts of interest

The authors declare no competing financial interests.

### Acknowledgments

Work at the Center for Nanoscale Materials, Advanced Photon Source, and Electron Microscopy Center, was supported by the U.S. Department of Energy, Office of Science, Office of Basic Energy Sciences, under Contract No. DE-AC0206CH-11357. Support from the Vehicle Technologies Program at the U.S. Department of Energy, Office of Energy Efficiency and Renewable Energy is gratefully acknowledged. The work in the Balandin group was supported, in part, by the National Science Foundation grants ECCS 1549942 and CMMI 1404967.

### References

- [1] M.S. Whittingham, Electrical energy storage and intercalation chemistry, *Science* 192 (4244) (1976) 1126–1127.
- [2] N. Nitta, F. Wu, J.T. Lee, G. Yushin, Li-ion battery materials: present and future, *Mater. Today* 18 (5) (2015) 252–264.
- [3] L. Lu, X. Han, J. Li, J. Hua, M. Ouyang, A review on the key issues for lithium-ion battery management in electric vehicles, *J. Power Sources* 226 (Supplement C) (2013) 272–288.
- [4] J.B. Goodenough, K.-S. Park, The Li-Ion rechargeable battery: a perspective, *J. Am. Chem. Soc.* 135 (2013) 1167–1176.
- [5] V. Etacheri, R. Marom, R. Elazari, G. Salitra, D. Aurbach, Challenges in the development of advanced Li-ion batteries: a review, *Energy Environ. Sci.* 4 (2011) 3243–3262.
- [6] B. Dunn, H. Kamath, J.-M. Tarascon, Electrical energy storage for the grid: a battery of choices, *Science* 334 (6058) (2011) 928–935.
- [7] Z. Chen, P.-C. Hsu, J. Lopez, Y. Li, J.W.F. To, N. Liu, C. Wang, Sean C. Andrews, J. Liu, Y. Cui, Z. Bao, Fast and reversible thermoresponsive polymer switching materials for safer batteries, *Nat. Energy* 1 (2016) 15009.
- [8] O.S. Burheima, M.A. Onsrud, J.G. Pharoah, F. Vullum-Bruer, P.J.S. Vied, Thermal conductivity, heat sources and temperature profiles of Li-Ion batteries, *ECS Trans.* 58 (48) (2014) 145–171.
- [9] D.R. Linden, T. B., *Handbook of Batteries*, third ed., McGraw-Hill, New York, 2002.
- [10] R. Spotnitz, J. Franklin, Abuse behavior of high-power, lithium-ion cells, *J. Power Sources* 113 (2003) 81–100.
- [11] J. Vetter, P. Novák, M.R. Wagner, C. Veit, K.C. Möller, J.O. Besenhard, M. Winter, M. Wohlfahrt-Mehrens, C. Vogler, A. Hammouche, Ageing mechanisms in lithium-ion batteries, *J. Power Sources* 147 (1) (2005) 269–281.
- [12] T.M. Bandhauer, S. Garimella, T.F. Fuller, A critical review of thermal issues in lithium-ion batteries, *J. Electrochem. Soc.* 158 (3) (2011) R1–R25.
- [13] P. Ramadass, B. Haran, P.M. Gomadam, R. White, B.N. Popov, Development of first principles capacity fade model for Li-Ion cells, *J. Electrochem. Soc.* 151 (2) (2004) A196–A203.
- [14] X.-B. Cheng, M.-Q. Zhao, C. Chen, A. Pentecost, K. Maleski, T. Mathis, X.-Q. Zhang, Q. Zhang, J. Jiang, Y. Gogotsi, Nanodiamonds suppress the growth of lithium dendrites, *Nat. Commun.* 8 (1) (2017) 336.
- [15] N. Williard, W. He, C. Hendricks, M. Pecht, Lessons learned from the 787 dreamliner issue on lithium-ion battery reliability, *Energies* 6 (9) (2013) 4682.
- [16] G.G. Amatucci, C.N. Schmutz, A. Blyr, C. Sigala, A.S. Godz, D. Larcher, J.M. Tarascon, Materials' effects on the elevated and room temperature performance of LiMn<sub>2</sub>O<sub>4</sub> Li-ion batteries, *J. Power Sources* 69 (1) (1997) 11–25.
- [17] S.S. Zhang, K. Xu, T.R. Jow, Electrochemical impedance study on the low temperature of Li-ion batteries, *Electrochim. Acta* 49 (7) (2004) 1057–1061.
- [18] Y. Ji, Y. Zhang, C.-Y. Wang, Li-ion cell operation at low temperatures, *J. Electrochem. Soc.* 160 (4) (2013) A636–A649.
- [19] J.M. Tarascon, M. Armand, Issues and challenges facing rechargeable lithium batteries, *Nature* 414 (2001) 359.
- [20] S.A. Khateeb, S. Amiruddin, M. Farid, J.R. Selman, S. Al-Hallaj, Thermal management of Li-ion battery with phase change material for electric scooters: experimental validation, *J. Power Sources* 142 (1) (2005) 345–353.
- [21] V. Vishwakarma, C. Waghele, Z. Wei, R. Prasher, S.C. Nagpure, J. Li, F. Liu, C. Daniel, A. Jain, Heat transfer enhancement in a lithium-ion cell through improved material-level thermal transport, *J. Power Sources* 300 (2015) 123–131.
- [22] F.-Y. Su, L.-Q. Dai, X.-Q. Guo, L.-J. Xie, G.-H. Sun, C.-M. Chen, Micro-structure evolution and control of lithium-ion battery electrode laminate, *J. Energy Storage* 14 (Part 1) (2017) 82–93.
- [23] H. Maleki, S.A. Hallaj, J.R. Selman, R.B. Dinwiddie, H. Wang, Thermal properties of lithium-ion battery and components, *J. Electrochem. Soc.* 146 (3) (1999) 947–954.
- [24] K. Evanoff, J. Khan, A.A. Balandin, A. Magasinski, W.J. Ready, T.F. Fuller, G. Yushin, Towards ultrathick battery electrodes: aligned carbon nanotube – enabled architecture, *Adv. Mater.* 24 (4) (2012) 533–537.
- [25] S.V. Garimella, A.S. Fleischer, J.Y. Murthy, A. Keshavarzi, R. Prasher, C. Patel, S.H. Bhavnani, R. Venkatasubramanian, R. Mahajan, Y. Joshi, B. Sankar, B.A. Myers, L. Chorosinski, M. Baelmans, P. Sathyamurthy, P.E. Raad, Thermal challenges in next-generation electronic systems, *IEEE Trans. Compon. Packag. Technol.* 31 (2008) 801–815.
- [26] P. Gotcu, W. Pfleging, P. Smyrek, H.J. Seifert, Thermal behaviour of Li<sub>x</sub>MeO<sub>2</sub> (Me = Co or Ni + Mn + Co) cathode materials, *Phys. Chem. Chem. Phys.* 19 (19) (2017) 11920–11930.
- [27] P. Gotcu, H.J. Seifert, Thermophysical properties of LiCoO<sub>2</sub>-LiMn<sub>2</sub>O<sub>4</sub> blended electrode materials for Li-ion batteries, *Phys. Chem. Chem. Phys.* 18 (15) (2016) 10550–10562.
- [28] J. Nanda, S.K. Martha, W.D. Porter, H. Wang, N.J. Dudney, M.D. Radin, D.J. Siegel, Thermophysical properties of LiFePO<sub>4</sub> cathodes with carbonized pitch coatings and organic binders: experiments and first-principles modeling, *J. Power Sources* 251 (Supplement C) (2014) 8–13.
- [29] A.A. Balandin, S. Ghosh, W. Bao, I. Calizo, D. Teweldebrhan, F. Miao, C.N. Lau, Superior thermal conductivity of single-layer graphene, *Nano Lett.* 8 (3) (2008) 902–907.
- [30] S.V. Kidalov, F.M. Shakhov, Thermal conductivity of diamond composites, *Materials* 2 (2009) 2467–2495.
- [31] A.A. Balandin, Thermal properties of graphene and nanostructured carbon materials, *Nat. Mater.* 10 (2011) 569–581.
- [32] J. Chen, J.H. Walther, P. Koumoutsakos, Covalently bonded graphene-carbon nanotube hybrid for high-performance thermal interfaces, *Adv. Funct. Mater.* 25 (2015) 7539–7545.
- [33] Z. Chen, J.W.F. To, C. Wang, Z. Lu, N. Liu, A. Chortos, L. Pan, F. Wei, Y. Cui, Z. Bao, A three-dimensionally interconnected carbon nanotube-conducting polymer hydrogel network for high-performance flexible battery electrodes, *Adv. Eng. Mater.* 4 (12) (2014). 1400207-n/a.
- [34] B. Zhao, L. Jiang, X. Zeng, K. Zhang, M.M.F. Yuen, J.-B. Xu, X.-Z. Fu, R. Sun, C.-P. Wong, A highly thermally conductive electrode for lithium ion batteries, *J. Mater. Chem.* 4 (38) (2016) 14595–14604.
- [35] Y. G.C.Fu, Z. Cui, Y. Li, W. Zhou, S. Xin, Y. Tang, J.B. Goodenough, Novel hydrogel-derived bifunctional oxygen electrocatalyst for rechargeable air cathodes, *Nano Lett.* 16 (10) (2016) 6516–6522.
- [36] J.D. Renteria, S. Ramirez, H. Malekpour, B. Alonso, A. Centeno, A. Zurutuza, A.I. Cocemasov, D.L. Nika, A.A. Balandin, Strongly anisotropic thermal conductivity of free-standing reduced graphene oxide films annealed at high temperature, *Adv. Funct. Mater.* 25 (29) (2015) 4664–4672.
- [37] G. Eda, G. Fanchini, M. Chhowalla, Large-area ultrathin films of reduced graphene oxide as a transparent and flexible electronic material, *Nat. Nanotechnol.* 3 (5) (2008) 270–274.
- [38] P. Kim, L. Shi, A. Majumdar, P.L. McEuen, Thermal transport measurements of individual multiwalled nanotubes, *Phys. Rev. Lett.* 87 (2001) 215502.
- [39] B. Marinho, M. Ghislandi, E. Tkalya, C.E. Koning, G. de With, Electrical conductivity of compacts of graphene, multi-wall carbon nanotubes, carbon black, and graphite powder, *Powder Technol.* 221 (2012) 351–358.
- [40] C. Ban, Z. Wu, D.T. Gillaspie, L. Chen, Y. Yan, J.L. Blackburn, A.C. Dillon, Nanostructured Fe<sub>3</sub>O<sub>4</sub>/SWNT electrode: binder-free and high-rate Li-Ion anode, *Adv. Mater.* 22 (20) (2010) E145–E149.
- [41] Y. Cheng, S. Lu, H. Zhang, C.V. Varanasi, J. Liu, Synergistic effects from graphene and carbon nanotubes enable flexible and robust electrodes for high-performance supercapacitors, *Nano Lett.* 12 (8) (2012) 4206–4211.
- [42] Y. Li, X. Lv, J. Li, High performance binderless TiO<sub>2</sub> nanowire arrays electrode



- for lithium-ion battery, *Appl. Phys. Lett.* 95 (11) (2009) 113102.
- [43] Z. Favors, H.H. Bay, Z. Mutlu, K. Ahmed, R. Ionescu, R. Ye, M. Ozkan, C.S. Ozkan, Towards scalable binderless electrodes: carbon coated silicon nanofiber paper via Mg reduction of electrospun SiO<sub>2</sub> nanofibers, *Sci. Rep.* 5 (2015) 8246.
- [44] C. Liu, C. Li, K. Ahmed, Z. Mutlu, C.S. Ozkan, M. Ozkan, Template free and binderless NiO nanowire foam for Li-ion battery anodes with long cycle life and ultrahigh rate capability, *Sci. Rep.* 6 (2016) 29183.
- [45] S. Ahmad, D. Copic, C. George, M. De Volder, Hierarchical assemblies of carbon nanotubes for ultraflexible Li-ion batteries, *Adv. Mater.* 28 (31) (2016) 6705–6710.
- [46] C. Zhang, J.-S. Yu, Morphology-tuned synthesis of NiCo<sub>2</sub>O<sub>4</sub>-coated 3D graphene architectures used as binder-free electrodes for lithium-ion batteries, *Chem. Eur. J.* 22 (13) (2016) 4422–4430.
- [47] K. Hasegawa, S. Noda, Lithium ion batteries made of electrodes with 99 wt% active materials and 1 wt% carbon nanotubes without binder or metal foils, *J. Power Sources* 321 (Supplement C) (2016) 155–162.
- [48] P. Goli, H. Ning, X. Li, C.Y. Lu, K.S. Novoselov, A.A. Balandin, Thermal properties of graphene–copper–graphene heterogeneous films, *Nano Lett.* 14 (3) (2014) 1497–1503.
- [49] P. Goli, S. Legedza, A. Dhar, R. Salgado, J. Renteria, A.A. Balandin, Graphene-enhanced hybrid phase change materials for thermal management of Li-ion batteries, *J. Power Sources* 248 (Supplement C) (2014) 37–43.
- [50] B. Koo, H. Xiong, M.D. Slater, V.B. Prakapenka, M. Balasubramanian, P. Podsiadlo, C.S. Johnson, T. Rajh, E.V. Shevchenko, Hollow iron oxide nanoparticles for application in lithium ion batteries, *Nano Lett.* 12 (5) (2012) 2429–2435.
- [51] B. Koo, P. Goli, A.V. Sumant, P.C.d.S. Claro, T. Rajh, C.S. Johnson, A.A. Balandin, E.V. Shevchenko, Toward lithium ion batteries with enhanced thermal conductivity, *ACS Nano* 8 (2014) 7202–7207.
- [52] B. Koo, S. Chattopadhyay, T. Shibata, V.B. Prakapenka, C.S. Johnson, T. Rajh, E.V. Shevchenko, Intercalation of sodium ions into hollow iron oxide nanoparticles, *Chem. Mater.* 25 (2) (2013) 245–252.
- [53] M. Shamsa, S. Ghosh, I. Calizo, V. Ralchenko, A. Popovich, A.A. Balandin, Thermal conductivity of nitrogenated ultrananocrystalline diamond films on silicon, *J. Appl. Phys.* 103 (8) (2008) 083538.
- [54] M. Shamsa, W.L. Liu, A.A. Balandin, C. Casiraghi, W.I. Milne, A.C. Ferrari, Thermal conductivity of diamond-like carbon films, *Appl. Phys. Lett.* 89 (16) (2006) 161921.
- [55] W.L. Liu, M. Shamsa, I. Calizo, A.A. Balandin, V. Ralchenko, A. Popovich, A. Saveliev, Thermal conduction in nanocrystalline diamond films: effects of the grain boundary scattering and nitrogen doping, *Appl. Phys. Lett.* 89 (17) (2006) 171915.
- [56] J. Cho, M.D. Losego, H.G. Zhang, H. Kim, J. Zuo, I. Petrov, D.G. Cahill, P.V. Braun, Electrochemically tunable thermal conductivity of lithium cobalt oxide, *Nat. Commun.* 5 (2014) 4035.
- [57] H. Im, J. Kim, Thermal conductivity of a graphene oxide–carbon nanotube hybrid/epoxy composite, *Carbon* 50 (15) (2012) 5429–5440.
- [58] C. Laurent, E. Flahaut, A. Peigney, The weight and density of carbon nanotubes versus the number of walls and diameter, *Carbon* 48 (10) (2010) 2994–2996.
- [59] S.S. Choi, H.S. Lim, Factors that affect cycle-life and possible degradation mechanisms of a Li-ion cell based on LiCoO<sub>2</sub>, *J. Power Sources* 111 (1) (2002) 130–136.
- [60] J. Cho, Y.J. Kim, T.-J. Kim, B. Park, Zero-strain intercalation cathode for rechargeable Li-ion cell, *Angew. Chem. Int. Ed.* 40 (2001) 3367–3369.
- [61] Z. Chen, J.R. Dahn, Effect of a ZrO<sub>2</sub> coating on the structure and electrochemistry of Li x CoO<sub>2</sub> when cycled to 4.5 V, *Electrochem. Solid State Lett.* 5 (10) (2002) A213–A216.
- [62] J. Cho, Y.J. Kim, B. Park, Novel LiCoO<sub>2</sub> cathode material with Al<sub>2</sub>O<sub>3</sub> coating for a Li ion cell, *Chem. Mater.* 12 (2000) 3788–3791.
- [63] M. Jo, S. Jeong, J. Cho, High power LiCoO<sub>2</sub> cathode materials with ultra energy density for Li-ion cells, *Electrochem. Commun.* 12 (7) (2010) 992–995.
- [64] H.-M. Cheng, F.-M. Wang, J.P. Chu, R. Santhanam, J. Rick, S.-C. Lo, Enhanced cycleability in lithium ion batteries: resulting from atomic layer deposition of Al<sub>2</sub>O<sub>3</sub> or TiO<sub>2</sub> on LiCoO<sub>2</sub> electrodes, *J. Phys. Colloid Chem.* 116 (14) (2012) 7629–7637.
- [65] G.T.-K. Fey, T.P. Kumar, Long-cycling coated LiCoO<sub>2</sub> cathodes for lithium batteries - a review, *J. Ind. Eng. Chem.* 10 (2004) 1090–1103.
- [66] J. Cho, Y.J. Kim, B. Park, LiCoO<sub>2</sub> cathode material that does not show a phase transition from hexagonal to monoclinic phase, *J. Electrochem. Soc.* 148 (10) (2001) A1110–A1115.
- [67] J.B. Dunn, L. Gaines, M. Barnes, J. Sullivan, M. Wang, *Materials and Energy Flows in the Materials Production, Assembly, and End-of-life Stages of the Automotive Lithium-ion Battery Life Cycle*, 2012. <http://www.osti.gov/bridge>.
- [68] M. Singh, J. Kaiser, H. Hahn, Thick electrodes for high energy lithium ion batteries, *J. Electrochem. Soc.* 162 (7) (2015) A1196–A1201.
- [69] Y.-K. Sun, S.-T. Myung, B.-C. Park, J. Prakash, I. Belharouak, K. Amine, High-energy cathode material for long-life and safe lithium batteries, *Nat. Mater.* 8 (4) (2009) 320–324.
- [70] M. Sathiyaa, K. Ramesha, G. Rousse, D. Foix, D. Gonbeau, A.S. Prakash, M.L. Doublet, K. Hemalatha, J.M. Tarascon, High performance Li<sub>2</sub>Ru<sub>1–y</sub>MnyO<sub>3</sub> (0.2 ≤ y ≤ 0.8) cathode materials for rechargeable lithium-ion batteries: their understanding, *Chem. Mater.* 25 (7) (2013) 1121–1131.